

Survival of Head and Neck Cancer Cells Relies upon LZK Kinase-Mediated Stabilization of Mutant p53

Zoe C. Edwards¹, Eleanor W. Trotter¹, Pedro Torres-Ayuso^{1,2}, Phil Chapman³, Henry M. Wood⁴, Katherine Nyswaner², and John Brognard^{1,2}



Abstract

Head and neck squamous cell carcinoma (HNSCC) includes epithelial cancers of the oral and nasal cavity, larynx, and pharynx and accounts for ~350,000 deaths per year worldwide. Smoking-related HNSCC is associated with few targetable mutations but is defined by frequent copy-number alteration, the most common of which is gain at 3q. Critical 3q target genes have not been conclusively determined for HNSCC. Here, we present data indicating that *MAP3K13* (encoding LZK) is an amplified driver gene in HNSCC. Copy-number gain at 3q resulted in increased

MAP3K13 mRNA in HNSCC tumor samples and cell lines. Silencing LZK reduced cell viability and proliferation of HNSCC cells with 3q gain but not control cell lines. Inducible silencing of LZK caused near-complete loss of colony-forming ability in cells harboring 3q gain. These results were validated *in vivo* by evidence that LZK silencing was sufficient to reduce tumor growth in a xenograft model of HNSCC. Our results establish LZK as critical for maintaining expression of mutant stabilized p53. *Cancer Res*; 77(18); 4961–72. ©2017 AACR.

Introduction

Head and neck squamous cell carcinoma (HNSCC) is driven by frequent copy-number alteration, the most common of which is gain of 3q, the long arm of chromosome 3 (1). Drivers identified on the 3q amplicon include *PIK3CA* (2, 3), *TP63* (4–6), and *SOX2* (7–9); however, targeting amplified *PIK3CA* has displayed limited success (10, 11), and small molecule inhibitors do not exist for *SOX2* or p63, thus additional drivers must be identified to improve outcomes for HNSCC patients. We investigated the kinase LZK (encoded by *MAP3K13*, a resident gene on the 3q amplicon) as a novel target because it was previously reported to regulate the JNK (12, 13) and NFκB (14) pathways, which can be protumorigenic. There are few studies describing the function of LZK, but a previous study demonstrated that LZK and its close family member DLK play a role in synaptic growth. Specifically, the DLK/LZK *Drosophila* homolog, *wallenda*, is required for synaptic overgrowth (15), and overexpression of LZK can promote

axon growth in neurons (16). In addition, DLK/LZK inhibitors have been developed and show activity in a Parkinson's disease mouse model (17).

Mutation or deletion of *TP53* (encoding p53) is a frequent and early event in the development of HNSCC (1). Wild-type p53 is a critical tumor suppressor; however, many *TP53* mutations produce a full-length protein, which is highly expressed in cancer cells (18). Several hotspot mutations have been identified and demonstrated to have oncogenic capabilities (reviewed in refs. 19 and 20), including the ability to transform p53-null cells and promote tumor growth in mice (21). Gain-of-function (GOF) p53 mutants are associated with antiapoptotic (22, 23), proliferative (24–26), and proinvasive phenotypes (25, 27), and can promote resistance to chemotherapy (24, 28). GOF p53 mutants have been shown to upregulate cyclins A and B1 (26), hTERT (29), MDR1 (21), NFκB2 (30), and MYC (31) and downregulate p21, PTEN, BAX (22), and caspase-3 (28). GOF p53 has also been shown to interact with and inhibit AMPK (27), and modulate chromatin regulatory factors, including MLL1, MLL2, and MOZ (32). GOF-mutant p53 is stabilized by tumor cell-specific factors (33), the mechanisms of which are not fully understood. Currently, no therapeutics have been specifically developed to suppress the expression of stabilized mutant p53; however, HSP90 inhibitors were previously shown to reduce expression of mutant p53 (23). Here, we describe LZK as essential to maintain proliferation of HNSCC cells with 3q gain, via promoting stability of GOF-mutant p53.

¹Signalling Networks in Cancer Group, Cancer Research UK Manchester Institute, The University of Manchester, Manchester, United Kingdom. ²Laboratory of Cell and Developmental Signaling, National Cancer Institute at Frederick, Frederick, Maryland. ³Computational Biology Group, Cancer Research UK Manchester Institute, The University of Manchester, Manchester, United Kingdom. ⁴Leeds Institute of Cancer and Pathology, Wellcome Trust Brenner Building, St. James' University Hospital, Leeds, United Kingdom.

Note: Supplementary data for this article are available at Cancer Research Online (<http://cancerres.aacrjournals.org/>).

E.W. Trotter and P. Torres-Ayuso contributed equally to this article.

Corresponding Author: John Brognard, Center for Cancer Research, National Cancer Institute, Advanced Technology Research, Progress Drive, Frederick, MD 21701. Phone: 301-846-1163; Fax: 301-846-1251; E-mail: john.brognard@nih.gov

doi: 10.1158/0008-5472.CAN-17-0267

©2017 American Association for Cancer Research.

Materials and Methods

Plasmids and transfections

LZK cDNA was prepared from RNA extracted from 293T cells, *attB* flanking regions were added by PCR, and the BP clonase reaction used to insert LZK into pDONR221. From here the Invitrogen Gateway system was used for cloning into destination

vectors. FLAG-tagged (pReceiver-M12, GeneCopoeia) destination vector was converted into Gateway destination vector for use in transient overexpression assays. The pLenti6.3/TO/V5-DEST vector was used to generate stable overexpression. Mutations were introduced using a Site-Directed Mutagenesis Kit (Stratagene). Kinase dead (KD) construct used for LZK was a K195M mutant. For the shRNA-resistant LZK construct, mutations were as follows: g978t, t981c, a984g, t987a, c990g, t993c, and a996g.

293T, CAL33, and BEAS2B cells were transiently transfected using Attractene (Qiagen) according to manufacturer's protocol. BICR56 cells were transfected using Lipofectamine LTX & Plus reagent (Invitrogen) according to manufacturer's protocol. A pcDNA3.1(+) vector (Invitrogen) was used as an empty vector control where required. DharmaFECT1 (Thermo Scientific) was used for siRNA transfections. siRNA used for LZK was obtained from Origene and used at 10 nmol/L. Sequences were as follows: GGAACACGAUGAAUCAGAGACGGCG (siLZKA), GGCGAAU-AAUUUUAUACAUGGAAUTG (siLZKB), and AGAACAGAAUGA-GACCGAUUAUCAAG (siLZKC). siRNA to p53 was ordered from Santa Cruz (si-p53#1; sc-29435) and Cell Signaling Technology (si-p53#2; 6231) and used at 100 nmol/L. Nontargeting control siRNA was ordered from Dharmacon (D-001810-01-20) and used at the same concentration as siRNA to the appropriate target. Staurosporine was purchased from Cell Signaling Technology.

Cell culture

CAL33 (DMSZ, obtained October 2012) and 293T (ATCC, July 2012) cells were maintained in DMEM D6546 (Sigma) supplemented with 10% FBS (Labtech), 1% penicillin-streptomycin (pen-strep; Gibco), and 2 mmol/L GlutaMAX (Gibco). BICR6 (March 2015), BICR16 (January 2014), BICR22 (October 2013), and BICR56 (November 2012 and April 2014; all obtained from Public Health England) cells were grown in DMEM D6546 with 10% FBS, 1% pen-strep, 0.4 µg/mL hydrocortisone (Sigma), and 2 mmol/L GlutaMAX. MSK921 (MSKCC, July 2014) and BEAS2B (ATCC, October 2012) cells were maintained in RPMI 1640 + GlutaMAX (Gibco) with 10% FBS and 1% pen-strep. PE-CA/PJ15 (PJ15) and PE-CA/PJ34 (PJ34; both obtained January 2014 from Public Health England) were cultured in IDMEM with 10% FBS, 1% pen-strep, and 2 mmol/L GlutaMAX. DETROIT562 (ATCC, November 2014) cells were maintained in EMEM (ATCC) with 10% FBS and 1% pen-strep (Gibco). 293FT (Invitrogen, November 2011) were maintained in DMEM with 10% FBS, 4 mmol/L GlutaMAX, 1 mmol/L sodium pyruvate (Gibco), and 0.1 mmol/L NEAA (Gibco). OKF6/TERT2 cells (Harvard Skin Disease Research Center, June 2013) were seeded in K-sfm (Gibco) with accompanying supplements: 25 µg/mL bovine pituitary extract, 0.2 ng/mL EGF, 0.3 mmol/L CaCl₂, and 1% pen-strep. At 30% confluency, medium was changed for 1:1 K-sfm:DFK to allow growth to full confluence. DFK was composed of DMEM/F12 (Gibco) with 2 mmol/L GlutaMAX, 25 µg/mL bovine pituitary extract (Gibco), 0.2 ng/mL EGF (Gibco), 0.3 mmol/L CaCl₂ (Lonza), and 1% pen-strep. Incubation was at 37°C and 5% CO₂ for all cells. Cell lines in regular use were subject to authentication by yearly STR profiling (conducted by multiplex PCR assay by Applied Biosystems Ampflstr system). STR profiles were compared with ATCC and DMSZ databases. However, no profile was available for BICR6, BICR22, MSK921, or OKF6/TERT2 cell lines, and BICR16, PJ15, and PJ34 were only removed from freeze for a short time after receipt for collection of DNA and RNA so were not authenticated. 3q status of all HNSCC and immortalized

control cell lines were verified in-house. All cell lines were used in experiments for fewer than 20 passages (10 weeks) after thawing, before a fresh vial was taken from freeze. Cell lines in use were confirmed to be *mycoplasma*-negative every 1 to 2 months.

Generation of doxycycline-inducible knockdown cell lines

CAL33, BICR56, OKF6/TERT2, BEAS2B, DETROIT562, and BICR6 inducible knockdown cells were generated by Sirion Biotech. MSK921 and BICR22 were generated in-house using lentiviral particles provided by Sirion (generated by transfection of 293TN cells with expression vectors and lentiviral packaging plasmids). Transduction was at MOI 5 with 8 µg/mL polybrene. After 24 hours, the medium was replaced with fresh medium containing puromycin (Invitrogen) to select for cells that had been effectively transduced. shRNA sequences were: CGGAAT-GAACCTGTCTCTGAA (sh1), GATGTAGATTCTTCAGCCATT (sh2), and AAGAGCCGATATCGAAGCAAA (sh3). The lentiviral expression plasmid was pCLVi(3G)-MCS-Puro, which expresses a doxycycline-responsive transactivator and the shRNA from the same vector. Expression of the transactivator is constitutive, while expression of shRNA is dependent on a doxycycline-inducible promoter. Binding of doxycycline to the transactivator allows it to bind the doxycycline-inducible promoter and promote expression of the shRNA. Doxycycline (Sigma) was used at 1 µg/mL to induce knockdown of LZK.

Generation of tetracycline-inducible expression cell lines

The ViraPower HiPerform T-Rex Gateway Expression System (Invitrogen) was used to generate cells with tetracycline-inducible expression of LZK. Briefly, LZK (cloned into pLenti6.3/TO/V5-DEST vector) and pLenti3.3/TR (for tetracycline repressor expression) were transfected into 293FT cells using Lipofectamine2000 to generate lentiviral stock. Parental OKF6/TERT2 and BEAS2B cells were transduced with lentiviral stocks in a stepwise fashion and cell lines generated by antibiotic selection [Blasticidin (Invitrogen) and Geneticin (Gibco)]. Tetracycline (Invitrogen) was used at 1 µg/mL to induce expression of LZK.

RNA preparation

Forty-eight hours after treatment (transient transfection, tetracycline-induced overexpression, or doxycycline-induced knockdown), cells were lysed using RLT buffer (Qiagen) with 1% v/v 2-mercaptoethanol (BioRad). Removal of genomic DNA and preparation of RNA was conducted using an RNeasy kit (Qiagen) according to the manufacturer's protocol. The quantity of RNA was determined using a NanoDrop ND-1000 spectrophotometer (NanoDrop Technologies).

RT-PCR

RT-PCR was performed using SuperScript III One-Step RT-PCR kit (Invitrogen). Primers used were as follows: AACTGATTC-GAAGGCGCAGA (LZK forward); GGGCGTTTTCCAAGAGAGGA (LZK reverse); CCATGGAGAAGGCTGGGG (GAPDH forward); GTCCACCACCCTGTTGCTGTA (GAPDH reverse). The cycling conditions for PCR were as follows: cDNA synthesis and pre-denaturation (1 cycle at 55°C for 30 minutes followed by 94°C for 2 minutes); PCR amplification (25 cycles of denaturing at 94°C for 15 seconds, annealing at 55°C for 30 seconds and extension at 68°C for 60 seconds) and a final extension at 68°C for 5 min. PCR products were resolved on 2% agarose gel and visualized with Nancy-520 (Sigma) DNA gel stain under UV light.

qRT-PCR

The Power SYBR Green RNA-to- C_T 1-Step Kit (Applied Biosystems) was used for qRT-PCR. Primers used were as follows: CCTTTGTCGGGAAGTCCCAAATGTC (LZK forward); GAAGG-TATTGGGATTGAGCTTGGTG (LZK reverse); CCAACCGCGA-GAAGATGA (ACTB forward); CCAGAGGCGTACAGGGATAG (ACTB reverse); TTCTGGCCTGGAGGCTATC (B2M forward); TCAGGAAATTTGACTTCCATTC (B2M reverse). Samples were run on an ABI 7900 HT real-time PCR instrument, with the following program: reverse transcription (48°C, 30 minutes), activation of DNA polymerase (95°C, 10 minutes), PCR amplification (40 cycles of denaturing at 95°C for 15 seconds and annealing/extension at 60°C for 1 minutes). SDS software was used to compute C_T values. Graphs display relative expression of *MAP3K13* compared with a reference gene and a control sample as stated in the relevant figure legend.

Protein lysate preparation and immunoblots

After appropriate treatment time, cells were lysed on ice with Triton X-100 lysis buffer (Cell Signaling Technology) supplemented with protease inhibitor tablet (Roche). Antibodies used were as follows: pJNK(T183/Y185), p-p53(S392), GAPDH, pIKB α (S32), pAMPK α (T172), AMPK α , p21, anti-rabbit, anti-mouse (Cell Signaling Technology), α -tubulin, Flag M2 (Sigma), p53 (Santa Cruz), LZK (abcam), p-p38(T180/Y182) (Genway), MDM2 (Millipore), and MDM4 (Bethyl laboratories).

Phosphoarrays

Two phosphoarrays were used: a phospho-kinase array and a MAPK array (both from R&D Systems). Samples were lysed 48 hours after induction by tetracycline or doxycycline as appropriate. Protocols were as per manufacturer's instructions.

MTT cell viability assays

Cells were seeded into 96-well plates in triplicate. For transient knockdown, cells were transfected at the same time as seeding and analyzed 72 hours later. For inducible knockdown, doxycycline was added into the medium the following day and analyzed 72 hours later. MTT Kit (Sigma) was used to assess viability, using protocol as per manufacturer's instructions.

MTS cell viability assays

For MTS assays, Cell Titer 96 Aqueous One Solution cell proliferation assay (Promega) was used, following the manufacturer's protocol. Briefly, cells were reverse transfected with the corresponding p53 siRNA or negative control. Twenty-four hours later, cells were collected and seeded into 96-well plates in triplicate for MTS assay and 6-well plates for protein extraction. Doxycycline was added where appropriate and cells were incubated for 72 hours. MTS was added, incubated for 4 hours, and absorbance measured at 490 nm.

Cell proliferation assays

Cells were seeded into 96-well plates in triplicate, and doxycycline added into the medium the following day. Cells were treated for 48 hours before incubation with BrdUrd label for a further 24 hours prior to analysis by Calbiochem kit according to the manufacturer's instructions.

Relative cell density assays

Crystal violet assays were used to assess relative cell growth and survival after knockdown. For transient knockdown, cells were transfected at the same time as seeding and analyzed 72 hours later. For inducible knockdown, cells were seeded into 6-well plates in triplicate, treated with doxycycline the following day, and plates analyzed after 72 hours of treatment. Cells were then washed with PBS and fixed in ice-cold methanol, before staining with 0.5% Crystal violet in 25% methanol. For quantification, Crystal violet stain was dissolved in 10% acetic acid, incubated for 20 minutes with shaking, and read at 595 nm.

Colony formation assays

Cells were seeded into 6-well plates in triplicate at 300/well (BEAS2B and OKF6/TERT2 controls) or 1000/well (HNSCC cell lines), and treated with doxycycline the following day. Medium was refreshed every 48 hours for 14 days. Cells were stained with Crystal violet as described above.

Matrigel assay

The "3D on-top assay" (34) was used to assess growth in matrigel. Matrigel used was Growth Factor Reduced, Phenol Red-Free Basement Membrane Matrix from mouse EHS tumor (Corning). Matrigel was thawed at 4°C overnight. Plates and tips were pre-chilled prior to experiment, and the experiment was conducted on ice, except where specified. Twelve-well plates were coated with 200 μ L Matrigel and incubated at 37°C for 30 minutes. Cells were plated at 80,000/well in 0.5 mL medium and left to settle for 30 minutes at 37°C. 0.5 mL 5% Matrigel in medium was added gently to each well. The following day, cells were treated with 1 μ g/mL doxycycline where required. After 72 hours of treatment, plates were observed with an Axiovert 40 CFL Inverted Microscope, and photographs taken with the aid of AxioVision software. The "Color Threshold" tool in ImageJ was used to assess average colony size. Three images per condition were used for measurement, and average colony size was calculated for each condition.

Cell-cycle analysis

Cells were seeded into 6-well plates and treated with doxycycline the following day. After 48 hours, media with floating cells were collected to FACS tubes and plates trypsinized. Trypsinized cells were added to the FACS tubes with the media that were previously collected, and the tubes spun for 3 minutes at 2,000 rpm. Supernatant was discarded and 1 ml prechilled ethanol added dropwise to each tube while vortexing. Cells were kept at -20°C until analysis. A BD Cycletest Plus DNA Reagent Kit was used for sample staining, according to the manufacturer's instructions. Samples were run on a BD 3-color FACSCalibur, and results were analyzed using FlowJo.

Xenograft mouse model

Animal work was approved by the CRUK-MI Ethical Review Committee and was performed within the limits of a license granted by the Home Office according to the Animals (Scientific Procedures) Act 1986.

For inducible knockdown xenografts, 2×10^6 CAL33-sh1 cells were injected s.c. into the right posterior flanks of 6- to 8-week-old immunodeficient NOD-*scid* IL2Rgamma^{null} (NSG) female mice (32 mice, obtained from Charles River). Mice weighed between 19

and 24 g at the start of experiment. When tumors reached a volume of approximately 200 mm³, mice (10 per group) were randomly assigned to treatment with control or doxycycline diet (ssniff).

For parental cell xenografts, 2 × 10⁶ CAL33 cells were injected s.c. into the right posterior flanks of 8–10 week-old immunodeficient NSG female mice (8 mice; obtained from Charles River). Mice weighed between 20 and 24 g at the start of experiment. When tumors reached a volume of approximately 200 mm³, mice (4 per group) were assigned to treatment with control or doxycycline diet (ssniff).

Tumor formation was monitored every few days and tumor volume based on caliper measurements was calculated by the formula: tumor volume = (length × width × width)/2. Mice were culled when tumors reached maximum permitted volume 1,200 mm³ or after 5 weeks after injection of cells.

Statistical analysis

Error bars shown on graphs represent ± SEM. Two-tailed Welch *t*-test was used to assess the significance of differences between groups for assays. Analysis of variance (ANOVA) was conducted to assess the significance of differences in mRNA expression between groups based on GISTIC copy numbers.

Copy-number analysis

DNA from cell lines was prepared using a Qiagen Blood & Tissue kit, according to the manufacturer's instructions. Copy-number analysis was conducted by paired-end whole genome sequencing (2 × 100 bp reads) on an Illumina HiSeq 2000. Thirty million pairs per samples were generated, which gave ~2-fold coverage of the genome. The most common ploidy was defined as "normal" for the purposes of assessing copy-number gain and loss. Analysis was run according to previously published procedures (35). No viral genomes were detected in any sample, so cell lines were determined to be HPV-negative with 95% confidence (36).

Results

Amplification and expression of LZK/MAP3K13 in HNSCC

Examination of data from The Cancer Genome Atlas (TCGA) revealed that high-level amplification of *MAP3K13* was present in 20% of HNSCC tumors (Fig. 1A), while an additional 56% had copy-number gain (37). Furthermore, *MAP3K13* was within the top 100 most frequently amplified genes on chromosome 3 (Fig. 1B). Further analysis of TCGA tumor samples indicated that higher *MAP3K13* copy number was associated with significantly increased mRNA expression (Fig. 1C). In addition, data from the Cancer Cell Line Encyclopedia (CCLE) showed that upper aerodigestive tract (UADT) cell lines have the highest levels of *MAP3K13* mRNA compared with all other available cancer cell lines (Supplementary Fig. S1A; ref. 38).

LZK expression levels were assessed in a panel of HNSCC cell lines with 3q gain based on CCLE data. Control cell lines included BEAS2B immortalized bronchial epithelial cells and OKF6/TERT2 immortalized oral keratinocytes; both cell lines were diploid with no change at 3q (Fig. 1D). Copy-number analysis confirmed the presence of the 3q amplicon in almost all HNSCC cell lines tested (Fig. 1D). MSK921 was the only

HNSCC cell line tested that had no alteration at 3q (Fig. 1D). BICR22 was notable for the fact that its region of copy-number gain did not encompass *MAP3K13* (Fig. 1D). Therefore, BICR22 and MSK921 were chosen as control HNSCC cell lines. qRT-PCR showed that a majority of the cell lines with copy-number gain of *MAP3K13* had increased mRNA expression (Fig. 1E), confirming data observed for TCGA human primary tumor samples. Finally, Western blot analysis indicated increased LZK protein levels in cells with 3q gain compared with BEAS2B cells (Supplementary Fig. S1B).

LZK knockdown by siRNA reduces viability of HNSCC cells with copy-number gain

To determine whether LZK is important for maintaining tumorigenic phenotypes, siRNA-mediated knockdown was conducted. Three individual siRNAs effectively depleted LZK protein levels in CAL33 and BICR56 HNSCC cells, and in OKF6/TERT2 and BEAS2B control lines (Fig. 2A). All three LZK siRNAs caused a highly significant reduction in viability in CAL33 and BICR56 cells, but had no effect on BEAS2B or OKF6/TERT2 cells (Fig. 2B). In addition, Crystal violet staining, which was used to assess relative cell growth and survival, showed that knockdown of LZK decreased the cell density of CAL33 and BICR56 cells (Fig. 2C and D). No effect was observed in OKF6/TERT2 controls, although a minor reduction in cell density was seen for BEAS2B cells with siLZKB and siLZKC (Fig. 2C and D).

LZK knockdown by doxycycline-inducible shRNA reduces viability, colony formation, and growth *in vivo* of HNSCC cells with 3q gain

To validate these data, HNSCC cells with doxycycline-inducible expression of shRNA targeting *MAP3K13* were generated (Fig. 3A and B). Induced knockdown of LZK led to a 40% to 50% reduction in viability of CAL33 and BICR56 cells, but had no significant effect on viability of MSK921 or BICR22 control cell lines that lack *MAP3K13* copy-number gain (Fig. 3C). Consistent with these results, there was a ~50% decrease in Crystal violet staining in CAL33 and BICR56 cells after doxycycline-induced LZK knockdown, but no effect on MSK921 or BICR22 cells (Supplementary Fig. S2A and S2B). To confirm these data in a 3D setting that more closely mimics the tumor microenvironment, cells were grown in Matrigel; colony sizes of CAL33 and BICR56 cells were reduced after LZK knockdown, whereas no significant effect was seen for control cell lines (Fig. 3D and E). Clonogenicity was then assessed; a near-complete ablation of colony forming ability was observed for CAL33 and BICR56 cells after depletion of LZK (Fig. 3F; Supplementary Fig. S2C). MSK921 cells showed a smaller reduction in colony formation after doxycycline treatment; this effect occurred at least in part due to the toxicity of doxycycline, which also affected the parental cell line (Fig. 3F; Supplementary Fig. S2C). Doxycycline has been reported to have toxic effects on some cell lines (39, 40), and this toxicity is likely more pronounced when cells are seeded at a low density (41), which could explain why these effects were not seen in short-term assays. LZK depletion did not suppress growth of BICR22 cells (Fig. 3F; Supplementary Fig. S2C).

Critically, reexpression of the sh1-resistant LZK construct into CAL33-sh1 and BICR56-sh1 cells fully or partially, respectively, rescued the effect of LZK knockdown on cell density,

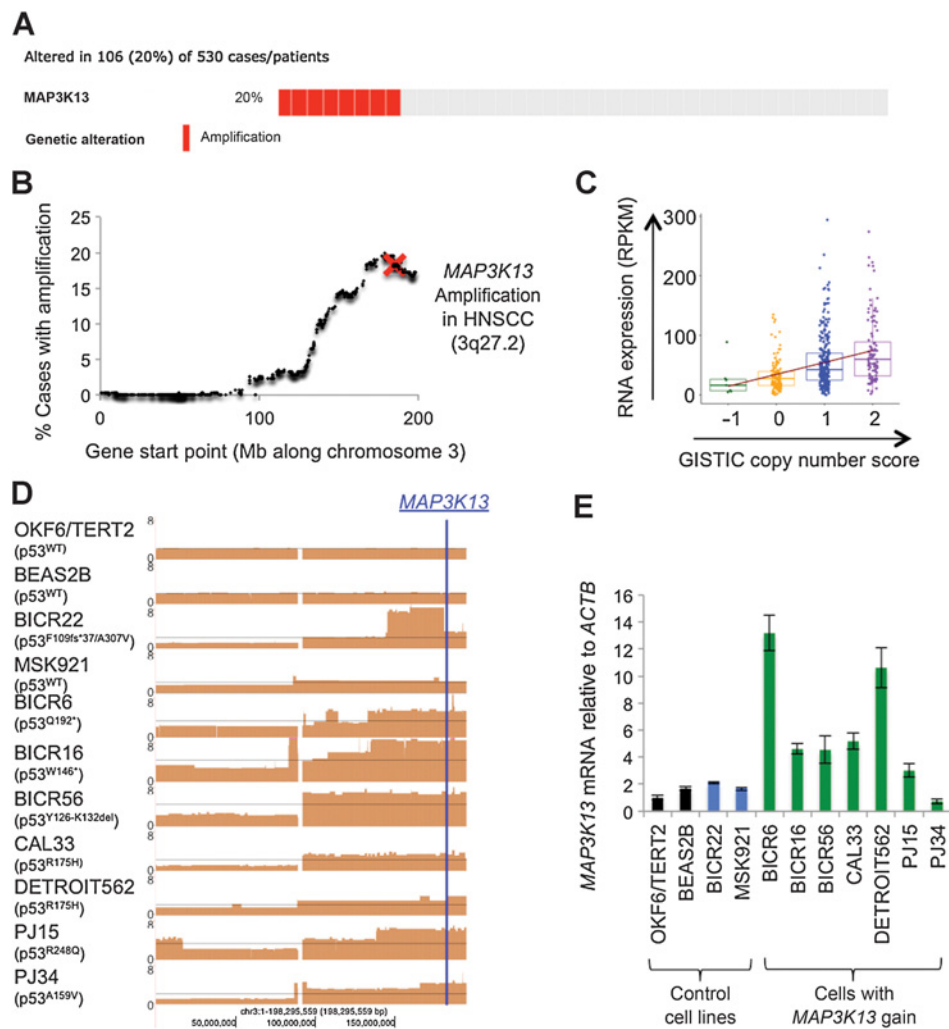


Figure 1.

Amplification and expression of *MAP3K13* (LZK) in HNSCC. **A**, Amplification of *MAP3K13* in 20% of HNSCC tumor samples from TCGA dataset. Graphic from cBio Portal. **B**, Graph representing percentage of HNSCC patients with amplification of each gene on chromosome 3, according to TCGA. *MAP3K13* is marked with a red cross. **C**, Increased copy number of *MAP3K13* leads to an increase in mRNA expression levels. RNA-seq expression data and GISTIC copy-number scores were extracted from the cBio portal. Box plots compare expression of *MAP3K13* across different GISTIC copy-number scores where -1 = loss of heterozygosity, 0 = diploid, 1 = gain, and 2 = amplification. ANOVA P value $2.3e - 11$. **D**, Copy-number gain of *MAP3K13* in HNSCC cell lines. Copy-number analysis was conducted by whole genome sequencing to determine which cell lines harbored the 3q amplicon. Data for chromosome 3 are shown. Most HNSCC cell lines have amplification of 3q (as compared with the overall average ploidy of each cell line, shown by blue y-indicator line), whereas control cell lines do not (BEAS2B immortalized bronchial epithelial cells, OKF6/TERT2 immortalized oral keratinocytes, and MSK921 HNSCC cells). Mutational status of p53 is indicated underneath each cell line. **E**, qRT-PCR shows increased *MAP3K13* mRNA expression in HNSCC lines with 3q copy-number gain relative to controls. Results were normalized to *ACTB* (β -actin) control gene and then to OKF6/TERT2 control cell line. Black, immortalized control cells; blue, HNSCC cells without *MAP3K13* gain; green, HNSCC cells with *MAP3K13* gain.

confirming that these effects were specific to LZK depletion (Fig. 4A). LZK knockdown was then conducted in additional control and HNSCC cell lines (Fig. 4B). shRNA-mediated depletion of LZK resulted in a significant reduction in colony formation in two additional HNSCC lines with 3q gain (BICR6 and DETROIT562), but not in BEAS2B or OKF6/TERT2 immortalized control cell lines (Fig. 4C and D). To determine the importance of LZK in vivo, we established a murine xenograft model using the CAL33-sh1 cell line. There was a significant reduction in tumor growth of $39\% \pm 16\%$ upon doxycycline treatment (Fig. 4E; note doxycycline diet had no significant

effect on parental CAL33 xenografts (Supplementary Fig. S3A). These results highlight the importance of LZK as a regulator of viability in HNSCC.

LZK knockdown by doxycycline-inducible shRNA reduces proliferation and cell-cycle progression of HNSCC cells with copy-number gain

Phenotypic assays were then carried out to investigate potential mechanisms of reduced viability. BrdUrd assays showed that depletion of LZK significantly reduced proliferation of CAL33 and BICR56 cells, while no effects were observed in

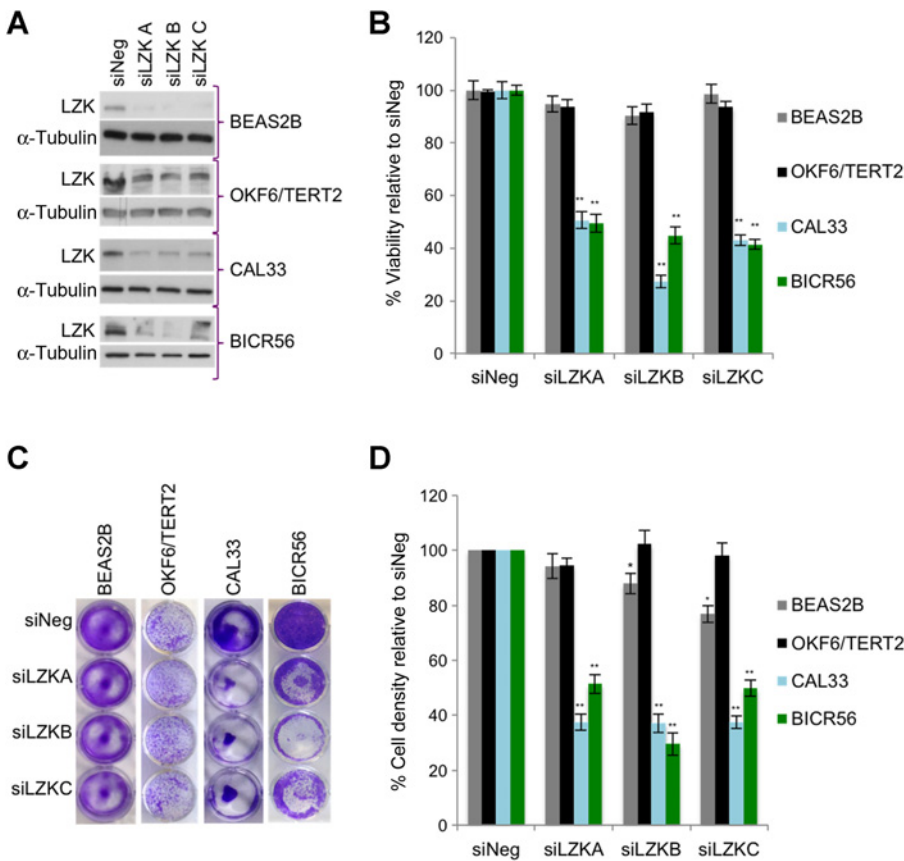


Figure 2. LZK knockdown by siRNA reduces relative cell density and viability of HNSCC cells with copy-number gain. **A**, LZK is knocked down in HNSCC and immortalized control cell lines by three separate siRNAs. Cells were reversely transfected for 24 hours (CAL33 and BICR56) or 48 hours (BEAS2B) with 10 nmol/L LZK or nontargeting control siRNA. Forward transfection for 72 hours was used for OKF6/TERT2 cells. **B**, Knockdown of LZK reduces viability of CAL33 and BICR56 HNSCC cells, but has no effect on BEAS2B OKF6/TERT2 cells. Cells were transfected in triplicate and analyzed by MTT assay 72 hours later. Graph shows average of at least three independent experiments and error bars indicate \pm SEM. **, *t* test, $P < 0.005$ compared with relevant negative control result. Two-tailed Welch *t* test used. **C**, Knockdown of LZK reduces relative cell density of CAL33 and BICR56 cells as compared with BEAS2B and OKF6/TERT2 controls. Cells were incubated for 72 hours after transfection, fixed with methanol, and stained with Crystal violet solution. **D**, Crystal violet was solubilized in 10% acetic acid and read at 595 nm to quantify results. Results averaged from at least three independent experiments and expressed relative to siNeg. Error bars, \pm SEM. *, *t* test, $P < 0.05$ compared with relevant negative control result. **, *t* test, $P < 0.005$ compared with relevant negative control result. Two-tailed Welch *t* test used.

control cells (Fig. 5A). The decrease seen was to a similar extent as that observed in viability and density assays, suggesting that this proliferative decrease may be the main mechanism underpinning these effects. To confirm these results, propidium iodide staining was used to assess the effect of LZK knockdown on progression through the cell cycle. An increase in the percentage of cells in G₁ phase was observed for CAL33 and BICR56 inducible knockdown cells depleted of LZK, but not for MSK921 control cells (Fig. 5B; Supplementary Table S1). This correlated with an increase in G₁-S ratio, a measure of cell-cycle arrest, of approximately 3-fold for CAL33 and 2-fold for BICR56 (Fig. 5C). These data verify that LZK regulates HNSCC viability through regulation of the cell cycle. Additionally, PARP cleavage, a marker of apoptosis, was not observed after LZK knockdown (Supplementary Fig. S 3B), suggesting that LZK does not regulate cell death in HNSCC.

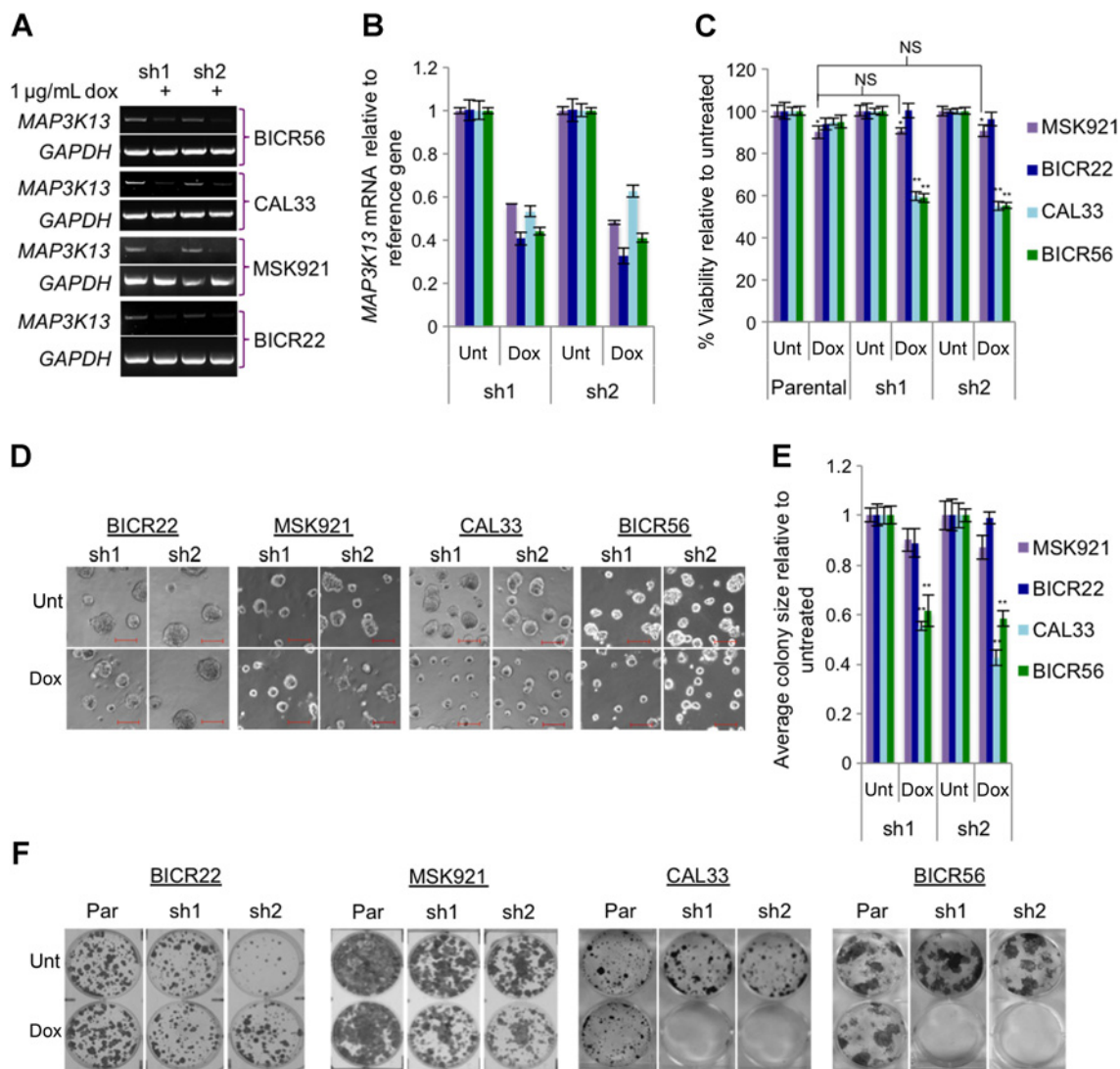
LZK knockdown leads to a reduction in levels of stabilized mutant p53

To identify pathways involved in the proproliferative effect of LZK, we monitored the activation status of pathways described to be activated by LZK: JNK (12, 13), p38 (13), and NFκB (Supplementary Fig. S4A; ref. 14). In overexpression assays we observed activation of JNK, but not p38 or NFκB (Supplementary Fig. S4B-S4F). However, in BICR56 and CAL33 cells, there was no decrease in phospho-JNK after transient or inducible knockdown (Supplementary Fig. S4G and S4H; note that minor reductions were observed for MSK921 cells, but this was also seen in parental MSK921 cells, suggesting that doxycycline may be responsible for

the reduction in pJNK in this cell line). This suggested that these pathways were not responsible for the reduced proliferation observed after LZK depletion.

To elucidate other pathways regulated by LZK, a phosphokinase array was conducted using CAL33-inducible knockdown cells. The most obvious differences seen were for three p53 phosphorylation sites (S15, S46, and S392; Fig. 6A). The phospho-p53 results were validated by Western blot for the S392 phospho-site; however, it was found that total p53 levels were reduced after LZK knockdown (Fig. 6B), accounting for the observed decrease in phospho-p53 at the three phospho-sites. Effects on p53 were then investigated in BICR56 cells; p53 levels were also markedly reduced in this cell line after depletion of LZK (Fig. 6C). No reductions in total p53 were observed in MSK921 cells (Fig. 6C; note doxycycline treatment alone did not alter p53 levels in parental cells; Supplementary Fig. S5A).

Notably, CAL33 has a known GOF mutation in p53 (R175H), so a decrease in total p53 would be expected to lead to reduced proliferation. In contrast, the MSK921 control cell line harbors wild-type p53. BICR56 has a mutation in p53 that leads to the exclusion of seven amino acids (Y126-K132) at the beginning of exon 5. To date, this mutant has not been characterized. Transient knockdown using siRNA was conducted to investigate the function of p53 in these cell lines (Supplementary Fig. S5B and S5C). Knockdown of p53 in CAL33 cells led to a 40% to 60% reduction in viability (Fig. 6D; Supplementary Fig. S5C), indicating that LZK primarily promotes viability by maintaining expression of GOF-mutant p53 in these cells. In BICR56 cells, knockdown of p53 led to a smaller but significant decrease in viability of 30% to 40%

**Figure 3.**

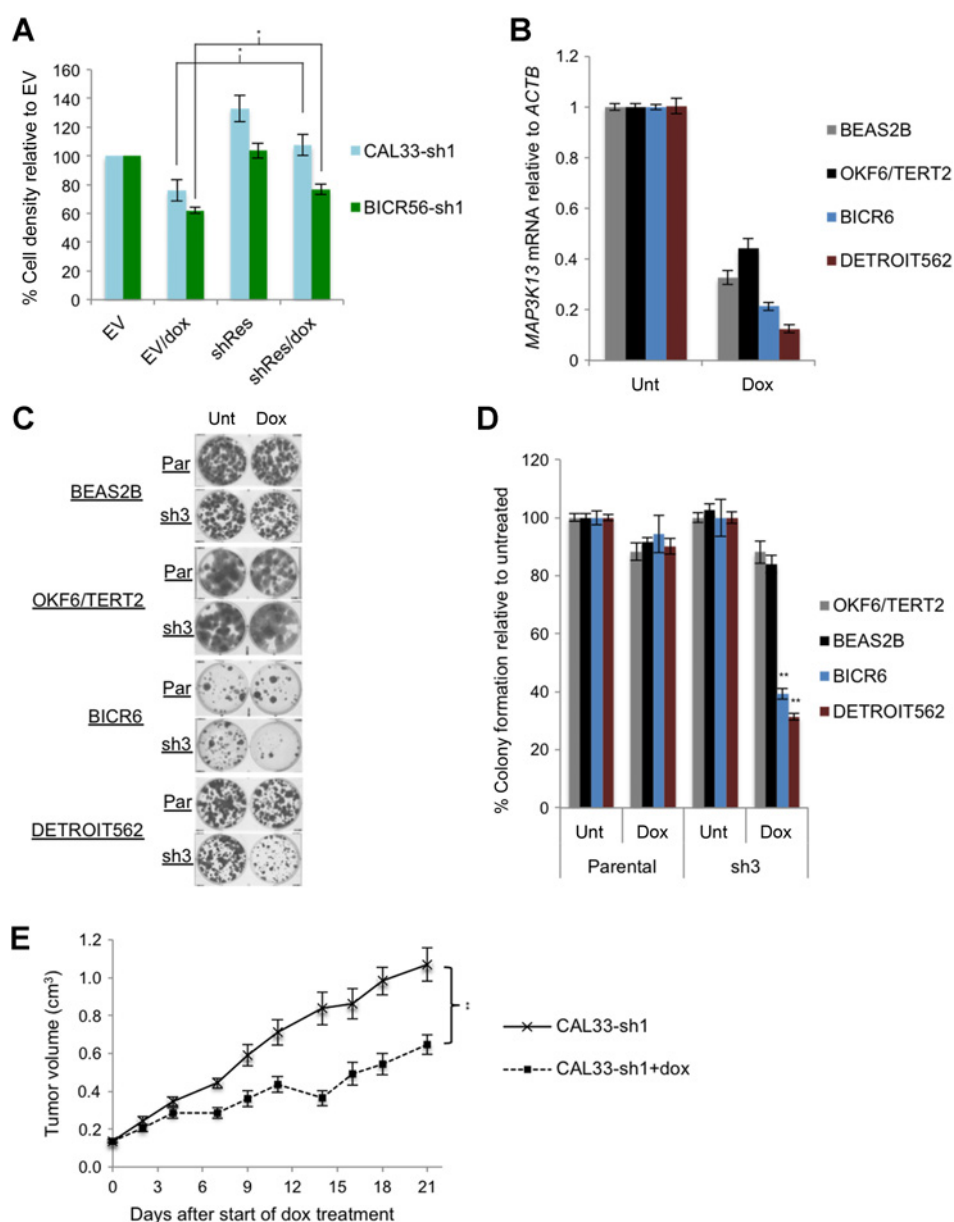
LZK knockdown by doxycycline-inducible shRNA reduces relative cell density, viability, and colony-forming potential of HNSCC cells with copy-number gain. **A**, Induction of shRNA by doxycycline reduces *MAP3K13* mRNA in BICR56, CAL33, BICR22, and MSK921-inducible knockdown cells. Knockdown was assessed by RT-PCR after 48-hour induction. **B**, qRT-PCR shows knockdown of *MAP3K13* in inducible knockdown lines after 48-hour doxycycline induction, as compared with control genes (*B2M* or *ACTB*). **C**, Knockdown of LZK reduces viability of CAL33 and BICR56 HNSCC cell lines, but has no effect on MSK921 or BICR22 cells. Cells were induced in triplicate and analyzed by MTT assay 72 hours later. Graph shows average of at least three independent experiments and error bars indicate \pm SEM. *, *t* test, $P < 0.05$ compared with relevant untreated control. **, *t* test, $P < 0.005$ compared with relevant untreated control result. NS, not significant. Two-tailed Welch *t* test used. **D**, Knockdown of LZK reduces cell growth of CAL33 and BICR56 cells in Matrigel as compared with MSK921 and BICR22 control cell lines. Cells were incubated for 72 hours after doxycycline treatment and visualized using an inverted light microscope. Scale bar, 100 μ m. **E**, The "Color Threshold" tool in ImageJ was used to assess average colony size of cells visualized in **D**. Three images per condition were used for measurement, and average colony size for each calculated. Values expressed relative to untreated control. Error bars, \pm SEM. **, *t* test, $P < 0.005$ compared with relevant negative control result. Two-tailed Welch *t* test used. **F**, Knockdown of LZK reduces colony-forming ability of CAL33 and BICR56 cells as compared with BICR22 and MSK921 controls. Cells were seeded at 1,000/well in 6-well plates in triplicate and treated with doxycycline for 14 days before fixing with methanol and staining with Crystal violet.

(Fig. 6D; Supplementary Fig. S5C), suggesting that these cells also require expression of stabilized mutant p53.

To determine if E3 ubiquitin ligases MDM2 and MDM4 were contributing to loss of expression of GOF-mutant p53, expression of these two proteins was monitored in cells depleted of LZK. Endogenous MDM4 was not detected in any of the HNSCC cell lines and endogenous MDM2 was only detected in the CAL33

cells (Supplementary Fig. S6A). There was no increase in MDM2 protein levels in CAL33 cells depleted of LZK (Supplementary Fig. S6B). Overall, these data indicate that regulation of these E3 ubiquitin ligases is not an underlying mechanism contributing to loss of p53 expression in HNSCC cells depleted of LZK.

To further understand the mechanism by which the LZK-GOF p53 pathway is promoting increased proliferation, we assessed

**Figure 4.**

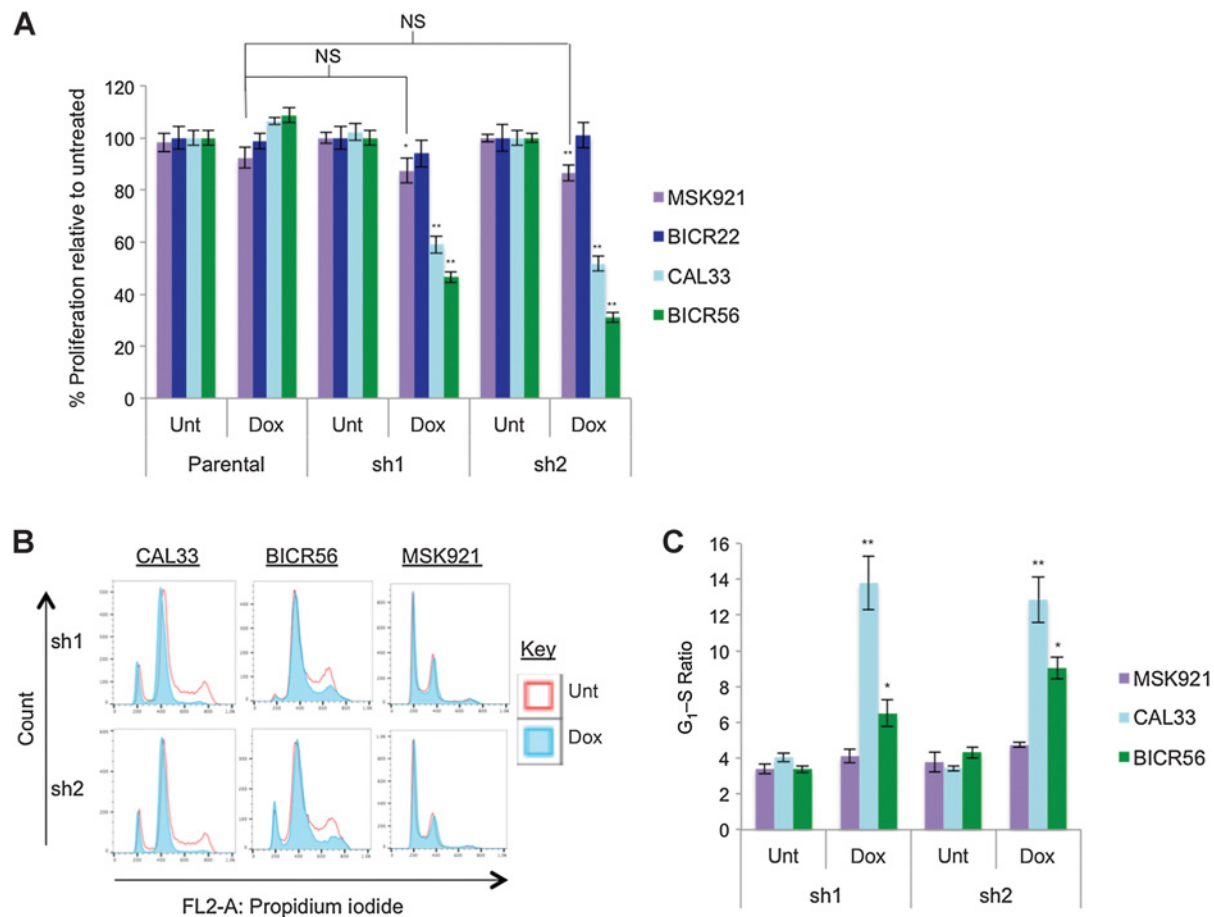
Confirmation of proliferative effect of amplified LZK *in vitro* and *in vivo*. **A**, Reduction in relative cell density after LZK knockdown is rescued by expression of shRNA-resistant LZK. Full rescue achieved for CAL33 and partial rescue for BICR56. Cells with inducible sh1 construct were transiently transfected 24 hours after seeding with FLAG-tagged shRNA-resistant LZK (shRes) or empty vector (EV) control. Eight hours after transfection, medium was changed and 1 μ g/mL doxycycline added where required. Cells were stained with Crystal violet 72 hours after transfection. *, Welch two-tailed *t* test, $P < 0.05$. **B**, qRT-PCR shows knockdown of *MAP3K13* in sh3 inducible knockdown lines after 48 hours doxycycline induction, as compared with *ACTB* reference gene. **C**, Doxycycline-induced knockdown of LZK reduces colony formation of additional HNSCC cell lines with 3q gain (BICR6 and DETROIT562), but not immortalized control cell lines. Cells were seeded in triplicate and treated with doxycycline for 2 weeks prior to Crystal violet staining. **D**, Quantification of results visualized in **C**. **, *t* test, $P < 0.005$ compared with corresponding doxycycline-treated parental cells. Two-tailed Welch *t* test used. **E**, Doxycycline-induced knockdown of LZK reduces tumor growth of CAL33 cells by 39% \pm 16%. A total of 2×10^6 CAL33 cells with inducible knockdown of LZK were engrafted in NSG mice. After tumor establishment, mice were randomized and treated with doxycycline or control diet. Tumor volume based on caliper measurements was calculated by the formula: tumor volume = (length \times width \times width)/2. Mean tumor volumes \pm SEM are shown ($n = 10$ mice/group); **, $P < 0.005$.

activation and expression of targets downstream of GOF-mutant p53 (22, 27). Depletion of LZK resulted in increased levels of p21 and phospho-AMPK α in CAL33 and BICR56 cells (Fig. 6E), consistent with previous reports that GOF-mutant p53 suppresses these downstream targets. These results highlight a novel signaling pathway where LZK is required to maintain expression of GOF-mutant p53, which regulates activation of AMPK and expression of p21. Finally, re-expression of shRNA-resistant LZK in CAL33 and BICR56 cells restored levels of mutant p53, demonstrating that this effect was specifically due to depletion of LZK (Fig. 6F).

Discussion

HNSCC accounts for approximately 600,000 cases and 350,000 deaths per year worldwide (42, 43). A majority of

patients present with stage III or IV disease, and, after treatment, 50% will have disease progression within 2 years (44, 45). Five-year survival rates for patients who present with advanced disease are under 50% (46). At present, the current treatment regimens for later stages involve chemotherapy and/or radiotherapy, which carry significant toxicities (45, 47). Chemotherapy or radiotherapy can be enhanced by combination with cetuximab, which targets EGFR, in advanced stages of the disease (48, 49). EGFR is overexpressed in \sim 90% of HNSCC patients; however, only a small subset (13%) of patients respond to cetuximab monotherapy (50). Additionally, the inclusion of cetuximab to a regimen of chemoradiotherapy was not found to have any additional benefit, regardless of EGFR expression levels (51). Cetuximab is the only FDA-approved targeted therapy for the treatment of HNSCC patients, and a recent review of current clinical trials for HNSCC indicated that a majority of trials are centered around EGFR

**Figure 5.**

LZK knockdown by doxycycline-inducible shRNA reduces proliferation and cell-cycle progression of HNSCC cells with copy-number gain. **A**, Knockdown of LZK reduces proliferation of CAL33 and BICR56 cells as compared with BICR22 and MSK921. Cells were incubated for 48 hours after doxycycline treatment, then BrdUrd label added for a further 24 hours before analysis. Graph shows average of at least three independent experiments and error bars indicate \pm SEM. For MSK921 control cells, minor but significant effect of doxycycline is seen for inducible knockdown cells, but this is not significant when compared with doxycycline-treated parental cells. *, t test, $P < 0.05$ compared with relevant untreated control. **, t test, $P < 0.005$ compared with relevant untreated control result. NS, not significant. Two-tailed Welch t test used. **B**, LZK knockdown leads to an increase in cells in G₁ phase in CAL33 and BICR56 cells, but not in MSK921 controls. Histograms show cell count versus FL2-A (propidium iodide) for inducible knockdown cells. Cells were induced with 1 μ g/mL doxycycline 24 hours after seeding and incubated for 48 hours before collection. Once stained, cells were analyzed on a 3-color FACSCalibur. **C**, G₁-S ratio is increased for CAL33 and BICR56 cells after doxycycline-induced LZK knockdown. Graph shows an average of at least three independent experiments and error bars indicate \pm SEM. *, t test, $P < 0.05$ compared with relevant untreated control. **, t test, $P < 0.005$ compared with relevant untreated control result. Two-tailed Welch t test used.

inhibitors, including gefitinib and erlotinib, in combination with chemotherapy and/or radiotherapy (43). This highlights the intense need for the development of new therapies for the treatment of this disease.

The development of novel therapies has been hampered by the relative rarity of targetable mutations in HNSCC. The exception is *PIK3CA*, which is mutated in \sim 20% of HNSCC samples (1, 10), representing a cohort of patients that may benefit from treatment with PI3K/AKT inhibitors. In addition, recent studies have indicated that inhibitors targeting the mTOR and ERK pathways hold promise for treatment of HNSCC patients, including patients positive for *PIK3CA* mutations (52–54).

Rather than targetable mutations, the most common genetic alterations in HNSCC are somatic copy-number alterations, the most frequent of which is copy-number gain at 3q (1). Multiple

genes on the 3q amplicon can promote tumorigenic phenotypes, including *PIK3CA* (2, 3), *TP63* (4–6), and *SOX2* (7–9), and detailed studies must be undertaken to define the contribution of the various genes on this amplicon to tumor initiation and maintenance. *MAP3K13* (LZK) is another resident gene of the 3q amplicon. Here, we have shown that knockdown of LZK reduced proliferation specifically in HNSCC cells with 3q gain, an effect that was rescued by reexpression of shRNA-resistant LZK. Our data identify LZK as novel genetic dependency in HNSCC tumors harboring the 3q amplicon, and suggest LZK as a potential therapeutic target in HNSCC. Future studies will explore the potential of LZK inhibitors for the treatment of head and neck cancers harboring the 3q amplicon, both alone and in combination with other inhibitors, for example, targeting PI3K, AKT, and mTOR.

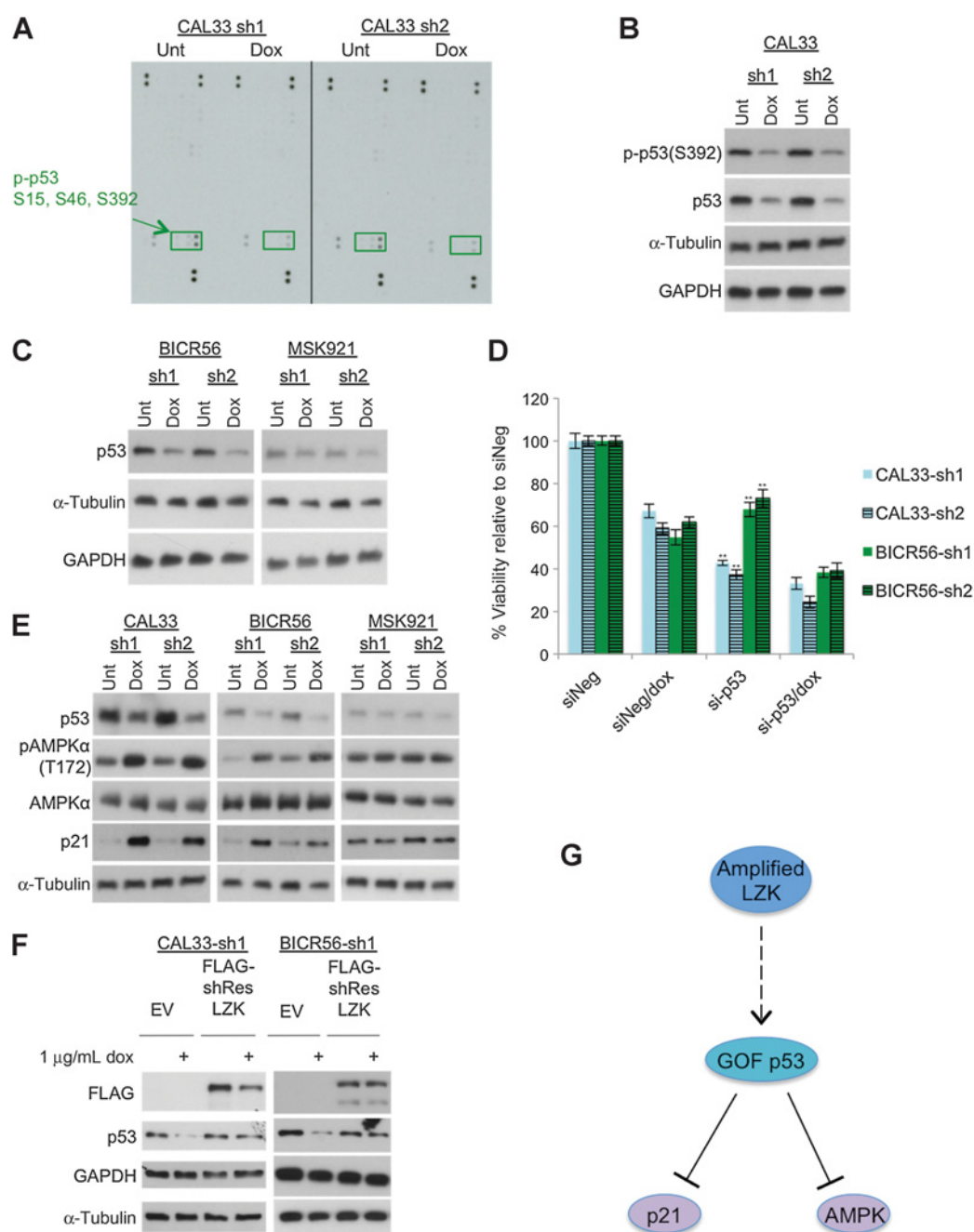


Figure 6.

LZK knockdown leads to a reduction in levels of stabilized mutant p53. **A**, Phosphoarray conducted after inducible knockdown of LZK in CAL33 cells indicates reduction in phospho-p53 (p-p53) at three different phosphorylation sites. Cells were treated with 1 μg/mL doxycycline for 48 hours before lysis. **B**, Validation of phosphoarray results in CAL33 cells. p-p53 reduction found to be due to a decrease in total p53 levels. Cells were treated with 1 μg/mL doxycycline for 48 hours before lysis. **C**, Extension of experiment to further inducible knockdown cell lines. BICR56 cells also show a clear decrease in p53 after LZK knockdown, while there is no effect in MSK921 cells. **D**, MTT assay to assess viability of cells after combination of doxycycline-induced LZK knockdown and transient p53 knockdown. p53 knockdown reduces viability of BICR56 and CAL33 cells, indicating that stabilized mutant p53 is required to maintain viability. Cells were reversely transfected in triplicate with 100 nmol/L siRNA to p53 (si-p53#1 used in this experiment) or nontargeting control, and induced with 1 μg/mL doxycycline (where appropriate) at the same time. MTT was read after 72 hours. Graph shows average of at least three independent experiments and error bars indicate ±SEM. **, Welch two-tailed *t* test, *P* < 0.005. **E**, Reduction in stabilized mutant p53 after LZK knockdown is associated with increased levels of pAMPKα and p21 in cells with 3q gain, but not MSK921 control cells. **F**, Western blots after rescue with shRNA-resistant LZK show partial rescue of p53 levels, confirming that this effect is specific to depletion of LZK. Cells with inducible sh1 construct were transiently transfected 24 hours after seeding with FLAG-tagged shRNA-resistant LZK (shRes) or empty vector (EV) control. Eight hours after transfection, medium was changed and 1 μg/mL doxycycline was added where indicated. Cells were lysed 48 hours after transfection. **G**, Model proposing the pathway by which amplified LZK promotes proliferation in HNSCC. LZK contributes to GOF mutant p53 stability, which promotes proliferation via regulation of its downstream targets, including p21 and AMPK.

Knockdown of LZK led to a reduction in protein levels of GOF-mutant p53 in cells with 3q gain; this was also rescued by reexpression of shRNA-resistant LZK. GOF-mutant p53 has been well documented to promote proliferation (24–26). In contrast to the wild-type protein, GOF-mutant p53 is found at constitutively high levels in cancer cells (18). However, the mutant proteins are not inherently more stable than the wild-type, as demonstrated by expression in normal tissue compared with tumor tissue in transgenic mice (33); this implies that GOF mutants are stabilized by tumor cell-specific factors. Our study highlights amplified LZK as one potential contributor to the maintenance of mutant p53 stability in HNSCC cells. When LZK was depleted, we also observed increases in levels of phospho-AMPK and p21, both of which are negatively regulated by GOF p53 (22, 27). Based on these observations, we propose a model whereby amplified LZK promotes stability of GOF-mutant p53, which in turn promotes proliferation of HNSCC cells via regulation of its downstream targets, including p21 and AMPK (Fig. 6G). The mechanism by which LZK stabilizes mutant p53 will be the focus of future studies.

In summary, our data indicate that LZK promotes proliferation in HNSCC with 3q copy-number gain, via maintaining expression of stabilized mutant p53. Enzymes that regulate stability of GOF-mutant p53 are attractive targets given the incidence of stabilized mutant p53 across all cancers. It was recently reported that over 11 million cancer patients live with stabilized mutant p53 (23); thus, LZK may represent a druggable genetic dependency for a subset of these patients where LZK is amplified.

Disclosure of Potential Conflicts of Interest

No potential conflicts of interest were disclosed.

References

1. Cancer Genome Atlas N. Comprehensive genomic characterization of head and neck squamous cell carcinomas. *Nature* 2015;517:576–82.
2. Yamamoto H, Shigematsu H, Nomura M, Lockwood WW, Sato M, Okumura N, et al. PIK3CA mutations and copy number gains in human lung cancers. *Cancer Res* 2008;68:6913–21.
3. Liang S, Yang N, Pan Y, Deng S, Lin X, Yang X, et al. Expression of activated PIK3CA in ovarian surface epithelium results in hyperplasia but not tumor formation. *PLoS One* 2009;4:e4295.
4. Rocco JW, Leong CO, Kuperwasser N, DeYoung MP, Ellisen LW. p63 mediates survival in squamous cell carcinoma by suppression of p73-dependent apoptosis. *Cancer Cell* 2006;9:45–56.
5. DeYoung MP, Johannessen CM, Leong CO, Faquin W, Rocco JW, Ellisen LW. Tumor-specific p73 up-regulation mediates p63 dependence in squamous cell carcinoma. *Cancer Res* 2006;66:9362–8.
6. Ramsey MR, Wilson C, Ory B, Rothenberg SM, Faquin W, Mills AA, et al. FGFR2 signaling underlies p63 oncogenic function in squamous cell carcinoma. *J Clin Invest* 2013;123:3525–38.
7. Bass AJ, Watanabe H, Mermel CH, Yu S, Perner S, Verhaak RG, et al. SOX2 is an amplified lineage-survival oncogene in lung and esophageal squamous cell carcinomas. *Nat Genet* 2009;41:1238–42.
8. Liu K, Jiang M, Lu Y, Chen H, Sun J, Wu S, et al. Sox2 cooperates with inflammation-mediated Stat3 activation in the malignant transformation of foregut basal progenitor cells. *Cell Stem Cell* 2013;12:304–15.
9. Lee SH, Oh SY, Do SI, Lee HJ, Kang HJ, Rho YS, et al. SOX2 regulates self-renewal and tumorigenicity of stem-like cells of head and neck squamous cell carcinoma. *Br J Cancer* 2014;111:2122–30.
10. Lui VW, Hedberg ML, Li H, Vangara BS, Pendleton K, Zeng Y, et al. Frequent mutation of the PI3K pathway in head and neck cancer defines predictive biomarkers. *Cancer Discov* 2013;3:761–9.
11. Mazumdar T, Byers LA, Ng PK, Mills GB, Peng S, Diao L, et al. A comprehensive evaluation of biomarkers predictive of response to PI3K inhibitors and of resistance mechanisms in head and neck squamous cell carcinoma. *Mol Cancer Ther* 2014;13:2738–50.
12. Sakuma H, Ikeda A, Oka S, Kozutsumi Y, Zanetta JP, Kawasaki T. Molecular cloning and functional expression of a cDNA encoding a new member of mixed lineage protein kinase from human brain. *J Biol Chem* 1997;272:28622–9.
13. Ikeda A, Hasegawa K, Masaki M, Moriguchi T, Nishida E, Kozutsumi Y, et al. Mixed lineage kinase LZK forms a functional signaling complex with JIP-1, a scaffold protein of the c-Jun NH(2)-terminal kinase pathway. *J Biochem* 2001;130:773–81.
14. Masaki M, Ikeda A, Shiraki E, Oka S, Kawasaki T. Mixed lineage kinase LZK and antioxidant protein-1 activate NF-kappaB synergistically. *Eur J Biochem* 2003;270:76–83.
15. Collins CA, Wairkar YP, Johnson SL, DiAntonio A. Highwire restrains synaptic growth by attenuating a MAP kinase signal. *Neuron* 2006;51:57–69.
16. Chen M, Geoffroy CG, Wong HN, Tress O, Nguyen MT, Holzman LB, et al. Leucine Zipper-bearing Kinase promotes axon growth in mammalian central nervous system neurons. *Sci Rep* 2016;6:31482.
17. Patel S, Cohen F, Dean BJ, De La Torre K, Deshmukh G, Estrada AA, et al. Discovery of dual leucine zipper kinase (DLK, MAP3K12) inhibitors with activity in neurodegeneration models. *J Med Chem* 2015;58:401–18.

Authors' Contributions

Conception and design: Z.C. Edwards, E.W. Trotter, J. Brognard

Development of methodology: Z.C. Edwards, E.W. Trotter, P. Torres-Ayuso, J. Brognard

Acquisition of data (provided animals, acquired and managed patients, provided facilities, etc.): Z.C. Edwards, E.W. Trotter, P. Torres-Ayuso, H.M. Wood, K. Nyswaner

Analysis and interpretation of data (e.g., statistical analysis, biostatistics, computational analysis): Z.C. Edwards, E.W. Trotter, P. Torres-Ayuso, P. Chapman, H.M. Wood, K. Nyswaner, J. Brognard

Writing, review, and/or revision of the manuscript: Z.C. Edwards, P. Torres-Ayuso, H.M. Wood, K. Nyswaner, J. Brognard

Administrative, technical, or material support (i.e., reporting or organizing data, constructing databases): J. Brognard

Study supervision: Z.C. Edwards, J. Brognard

Acknowledgments

We thank Lisa Doar and Adam Freestone from the BRU for technical support with the xenograft mouse model, MBCF for sequencing services, cell line authentication and mycoplasma testing, and Sudhakar Sahoo for copy-number analysis. Our thanks also go to Sirion Biotech for generating the doxycycline-inducible system.

Grant Support

This research was primarily supported by Cancer Research UK (Z.C. Edwards, E.W. Trotter, P. Torres-Ayuso, P. Chapman and J. Brognard), including under grant number C5759/A20971 (Z.C. Edwards and J. Brognard). P. Torres-Ayuso received funding from Fundación Ramón Areces. J. Brognard, P. Torres-Ayuso, and K. Nyswaner were funded by the National Cancer Institute, grant number ZIA BC 011691.

The costs of publication of this article were defrayed in part by the payment of page charges. This article must therefore be hereby marked *advertisement* in accordance with 18 U.S.C. Section 1734 solely to indicate this fact.

Received February 1, 2017; revised June 14, 2017; accepted July 21, 2017; published OnlineFirst July 31, 2017.

18. Burns JE, Baird MC, Clark LJ, Burns PA, Edington K, Chapman C, et al. Gene mutations and increased levels of p53 protein in human squamous cell carcinomas and their cell lines. *Br J Cancer* 1993;67:1274–84.
19. Oren M, Rotter V. Mutant p53 gain-of-function in cancer. *Cold Spring Harb Perspect Biol* 2010;2:a001107.
20. Muller PA, Vousden KH. p53 mutations in cancer. *Nat Cell Biol* 2013;15:2–8.
21. Dittmer D, Pati S, Zambetti G, Chu S, Teresky AK, Moore M, et al. Gain of function mutations in p53. *Nat Genet* 1993;4:42–6.
22. Vikhanskaya F, Lee MK, Mazzeletti M, Brogginini M, Sabapathy K. Cancer-derived p53 mutants suppress p53-target gene expression—potential mechanism for gain of function of mutant p53. *Nucleic Acids Res* 2007;35:2093–104.
23. Alexandrova EM, Yallowitz AR, Li D, Xu S, Schulz R, Proia DA, et al. Improving survival by exploiting tumour dependence on stabilized mutant p53 for treatment. *Nature* 2015;523:352–6.
24. Bossi G, Lapi E, Strano S, Rinaldo C, Blandino G, Sacchi A. Mutant p53 gain of function: reduction of tumor malignancy of human cancer cell lines through abrogation of mutant p53 expression. *Oncogene* 2006;25:304–9.
25. Li D, Marchenko ND, Schulz R, Fischer V, Velasco-Hernandez T, Talos F, et al. Functional inactivation of endogenous MDM2 and CHIP by HSP90 causes aberrant stabilization of mutant p53 in human cancer cells. *Mol Cancer Res* 2011;9:577–88.
26. Acin S, Li Z, Mejia O, Roop DR, El-Naggar AK, Caulin C. Gain-of-function mutant p53 but not p53 deletion promotes head and neck cancer progression in response to oncogenic K-ras. *J Pathol* 2011;225:479–89.
27. Zhou G, Wang J, Zhao M, Xie TX, Tanaka N, Sano D, et al. Gain-of-function mutant p53 promotes cell growth and cancer cell metabolism via inhibition of AMPK activation. *Mol Cell* 2014;54:960–74.
28. Wong RP, Tsang WP, Chau PY, Co NN, Tsang TY, Kwok TT. p53-R273H gains new function in induction of drug resistance through down-regulation of procaspase-3. *Mol Cancer Ther* 2007;6:1054–61.
29. Scian MJ, Stagliano KE, Deb D, Ellis MA, Carchman EH, Das A, et al. Tumor-derived p53 mutants induce oncogenesis by transactivating growth-promoting genes. *Oncogene* 2004;23:4430–43.
30. Scian MJ, Stagliano KE, Anderson MA, Hassan S, Bowman M, Miles MF, et al. Tumor-derived p53 mutants induce NF-kappaB2 gene expression. *Mol Cell Biol* 2005;25:10097–110.
31. Scian MJ, Stagliano KE, Ellis MA, Hassan S, Bowman M, Miles MF, et al. Modulation of gene expression by tumor-derived p53 mutants. *Cancer Res* 2004;64:7447–54.
32. Zhu J, Sammons MA, Donahue G, Dou Z, Vedadi M, Getlik M, et al. Gain-of-function p53 mutants co-opt chromatin pathways to drive cancer growth. *Nature* 2015;525:206–11.
33. Terzian T, Suh YA, Iwakuma T, Post SM, Neumann M, Lang GA, et al. The inherent instability of mutant p53 is alleviated by Mdm2 or p16INK4a loss. *Genes Dev* 2008;22:1337–44.
34. Lee GY, Kenny PA, Lee EH, Bissell MJ. Three-dimensional culture models of normal and malignant breast epithelial cells. *Nat Methods* 2007;4:359–65.
35. Gusnanto A, Wood HM, Pawitan Y, Rabbitts P, Berri S. Correcting for cancer genome size and tumour cell content enables better estimation of copy number alterations from next-generation sequence data. *Bioinformatics* 2012;28:40–7.
36. Conway C, Chalkley R, High A, MacLennan K, Berri S, Chengot P, et al. Next-generation sequencing for simultaneous determination of human papillomavirus load, subtype, and associated genomic copy number changes in tumors. *J Mol Diagn* 2012;14:104–11.
37. cBio Cancer Genomics Portal. <<http://www.cbioportal.org/public-portal/>>. Accessed 29th June 2015.
38. Cancer Cell Line Encyclopedia. <<http://www.broadinstitute.org/ccle/>>. Accessed 16th July 2015.
39. Xie J, Nair A, Hermiston TW. A comparative study examining the cytotoxicity of inducible gene expression system ligands in different cell types. *Toxicol In Vitro* 2008;22:261–6.
40. Shen LC, Chen YK, Lin LM, Shaw SY. Anti-invasion and anti-tumor growth effect of doxycycline treatment for human oral squamous-cell carcinoma—*in vitro* and *in vivo* studies. *Oral Oncol* 2010;46:178–84.
41. Ermak G, Cancasci VJ, Davies KJ. Cytotoxic effect of doxycycline and its implications for tet-on gene expression systems. *Anal Biochem* 2003;318:152–4.
42. Parkin DM, Bray F, Ferlay J, Pisani P. Global cancer statistics, 2002. *CA Cancer J Clin* 2005;55:74–108.
43. Du Y, Peyser ND, Grandis JR. Integration of molecular targeted therapy with radiation in head and neck cancer. *Pharmacol Ther* 2014;142:88–98.
44. Argiris A, Karamouzis MV, Raben D, Ferris RL. Head and neck cancer. *Lancet* 2008;371:1695–709.
45. Haddad RI, Shin DM. Recent advances in head and neck cancer. *N Engl J Med* 2008;359:1143–54.
46. Carvalho AL, Nishimoto IN, Califano JA, Kowalski LP. Trends in incidence and prognosis for head and neck cancer in the United States: a site-specific analysis of the SEER database. *Int J Cancer* 2005;114:806–16.
47. Mountzios G, Rampias T, Psyri A. The mutational spectrum of squamous-cell carcinoma of the head and neck: targetable genetic events and clinical impact. *Ann Oncol* 2014;25:1889–900.
48. Bonner JA, Harari PM, Giralt J, Azarnia N, Shin DM, Cohen RB, et al. Radiotherapy plus cetuximab for squamous-cell carcinoma of the head and neck. *N Engl J Med* 2006;354:567–78.
49. Vermorken JB, Mesia R, Rivera F, Remenar E, Kaweck i A, Rottey S, et al. Platinum-based chemotherapy plus cetuximab in head and neck cancer. *N Engl J Med* 2008;359:1116–27.
50. Vermorken JB, Trigo J, Hitt R, Koralewski P, Diaz-Rubio E, Rolland F, et al. Open-label, uncontrolled, multicenter phase II study to evaluate the efficacy and toxicity of cetuximab as a single agent in patients with recurrent and/or metastatic squamous cell carcinoma of the head and neck who failed to respond to platinum-based therapy. *J Clin Oncol* 2007;25:2171–7.
51. Ang KK, Zhang Q, Rosenthal DI, Nguyen-Tan PF, Sherman EJ, Weber RS, et al. Randomized phase III trial of concurrent accelerated radiation plus cisplatin with or without cetuximab for stage III to IV head and neck carcinoma: RTOG 0522. *J Clin Oncol* 2014;32:2940–50.
52. Wang Z, Martin D, Molinolo AA, Patel V, Iglesias-Bartolome R, Degese MS, et al. mTOR co-targeting in cetuximab resistance in head and neck cancers harboring PIK3CA and RAS mutations. *J Natl Cancer Inst* 2014;106: pii: dju215. doi: 10.1093/jnci/dju215.
53. Martin D, Abba MC, Molinolo AA, Vitale-Cross L, Wang Z, Zaida M, et al. The head and neck cancer cell oncogenome: a platform for the development of precision molecular therapies. *Oncotarget* 2014;5:8906–23.
54. Yamaguchi K, Iglesias-Bartolome R, Wang Z, Callejas-Valera JL, Amornphimoltham P, Molinolo AA, et al. A synthetic-lethality RNAi screen reveals an ERK-mTOR co-targeting pro-apoptotic switch in PIK3CA+ oral cancers. *Oncotarget* 2016;7:10696–709.